City Research Online

City, University of London Institutional Repository

Citation: Bianchi, G., Kovacevic, A., Cipollone, R., Murgia, S. & Contaldi, G. (2017). Grid generation methodology and CFD simulations in sliding vane compressors and expanders. IOP Conference Series: Materials Science and Engineering, 232(1), 012053. doi: 10.1088/1757-899x/232/1/012053

This is the accepted version of the paper.

This version of the publication may differ from the final published version.

Permanent repository link: https://openaccess.city.ac.uk/id/eprint/18565/

Link to published version: https://doi.org/10.1088/1757-899x/232/1/012053

Copyright: City Research Online aims to make research outputs of City, University of London available to a wider audience. Copyright and Moral Rights remain with the author(s) and/or copyright holders. URLs from City Research Online may be freely distributed and linked to.

Reuse: Copies of full items can be used for personal research or study, educational, or not-for-profit purposes without prior permission or charge. Provided that the authors, title and full bibliographic details are credited, a hyperlink and/or URL is given for the original metadata page and the content is not changed in any way.

City Research Online: http://openaccess.city.ac.uk/ publications@city.ac.uk

Grid generation methodology and CFD simulations in sliding vane compressors and expanders

Giuseppe Bianchi[1,2*], Sham Rane[1], Ahmed Kovacevic[1], Roberto Cipollone[3], Stefano Murgia[4], Giulio Contaldi[4]

[1]City University of London, United Kingdom
[2]Brunel University London, United Kingdom
[3]University of L'Aquila, Italy
[4]Ing. Enea Mattei S.p.A., Italy

*giuseppe.bianchi@brunel.ac.uk

Abstract. The limiting factor for the employment of advanced 3D CFD tools in the analysis and design of rotary vane machines is the unavailability of methods for generation of computational grids suitable for fast and reliable numerical analysis. The paper addresses this challenge presenting the development of an analytical grid generation for vane machines that is based on the user defined nodal displacement. In particular, mesh boundaries are defined as parametric curves generated using trigonometrical modelling of the axial cross section of the machine while the distribution of computational nodes is performed using algebraic algorithms with transfinite interpolation, post orthogonalisation and smoothing. Algebraic control functions are introduced for distribution of nodes on the rotor and casing boundaries in order to achieve good grid quality in terms of cell size and expansion. In this way, the moving and deforming fluid domain of the sliding vane machine is discretized and the conservation of intrinsic quantities in ensured by maintaining the cell connectivity and structure. For validation of generated grids, a mid-size air compressor and a small-scale expander for Organic Rankine Cycle applications have been investigated in this paper. Remarks on implementation of the mesh motion algorithm, stability and robustness experienced with the ANSYS CFX solver as well as the obtained flow results are eventually presented.

1. Introduction

Sliding vane machines are widely employed in industry nowadays. Typical applications where these devices are one of the leading technologies are compressed air systems, automotive thermal management (oil and cooling circuits), oil and gas applications. Nonetheless, unlike other positive displacement technologies that can rely on the design tools at the state of the art to improve and accelerate R&D and product development tasks, sliding vane machine designers cannot entirely benefit of these resources. In fact, the limiting factor for the employment of advanced 3D CFD tools in the analysis and design of rotary vane machines is the unavailability of methods for generation of computational grids suitable for fast and reliable numerical analysis.

In the literature, scientists and engineers have been investigating sliding vane devices both through experimental and numerical approaches. In particular, the modeling approaches that have been

developed mostly consider lumped parameter formulations of the conservation equations that undoubtedly benefit of reduced computational cost [1-4]. On the other hand, they do not allow to identify and optimize key issues in positive displacement machines such as the leakage paths, which in these models are schematized as equivalent orifices [5].

In recent years, the lack of a standardized and parameterized approach to discretize the fluid volume that stator, rotor and blades identify in a sliding vane machine has been started to be addressed by an increasing number of research works. Most of the developed procedures focused on expanders for waste heat to power generation based on an Organic Rankine Cycle architecture (ORC). For instance, Kolasiński and Błasiak performed experimental and numerical studies on a micro ORC sliding vane expander with circular stator and radial inlet and outlet ports [6] while Montenegro et al., investigated a sliding vane expander with an elliptic stator [7]. Working fluids were R123 and R245fa while CFD solvers employed in the afore mentioned studies were ANSYS CFX and OpenFOAM respectively. In both the research works, correction terms had to be introduced to deal with inaccuracies in the rotor grids. In addition to these research works, in commercial software such as Simerics PumpLinx or ANSYS there are templates on vane machines [8, 9]. However, they introduce a rather severe approximation when considering a flat blade profile. In fact, together with the stator, the tip of the blade forms a converging-diverging nozzle whose local curvature affect the overall leakage.

Among the available approaches for grid deformation, user defined nodal displacement was found to be the most suitable strategy to create a set of grids representing nodal locations for each time step externally, prior to the numerical flow solution in the calculation domain [10, 11]. User defined nodal displacement methodology was successfully applied to screw machine geometries and led to the development of two different strategies for grid generation. An algebraic approach was pursued by the research group at City, University of London [12] while a hybrid differential approach was considered at the University of Ghent [13]. Both the grid generation methods allowed to perform three-dimensional single and multi-phase simulations on screw compressors and expanders in recent years. In particular, the algebraic approach revealed more suitable for extension of grid generation to variable lead and variable profile rotors, while the hybrid differential approach resulted in better grid smoothing and adaptability to variety of rotor profiles such as hook and claw type positive displacement machines [11].

Regardless of the technology, positive displacement machines involve similar issues in the development of a deforming grid generation i.e. from clearance regions to the main core the aspect ratio of the geometry is 1000^{th} of order of magnitude, the computational cells need to maintain continuity through these highly deforming volumes and the cell structure needs to be maintained in order to avoid solution interpolation from one time step to the other. Hence, in the current study some of the algebraic algorithms developed for screw machinery have been applied to a sliding vane machine geometry and this led to the development of a novel general grid generation methodology. This innovative meshing procedure was tested with reference to two applications that highly differ for dimensions, operating parameters, working fluids and mode of operation. In particular, test cases presented in this paper are an oil injected air compressor and an ORC expander. After recalling the main steps of the grid generation for vane machines, the paper aims at highlighting similarities and differences occurred in the two simulation sets.

2. Grid Generation Procedure

In a sliding vane geometry, the working chamber is formed by the volume entrained between the housing, the rotor and the end plates. As the rotor carrying the set of vanes turns, each vane divides the full volume into successive chambers that undergo suction, compression/expansion and discharge phases. At the tip of each vane there is a thin gap that needs to be treated as the leakage. Even though the change in volume of this gap is very small compared to the core region, because of the eccentricity between rotor and stator, the relative shape of these gaps change with rotor positions. Altogether, the combined core and leakage gap form a O grid topology. Several algorithms for the structured meshing of O type domain topology are available in practice showed that algebraic algorithms with transfinite interpolation, post orthogonalisation and smoothing are the most efficient ones for applications like twin

screw compressors where a number of mesh files are required to be generated and supplied to the CFD solvers in order to treat mesh deformation [14]. Similar algebraic grid generation principle was used in this work for the vane geometry rotor domain mesh.

Flow chart in Figure 1 lists the main stages of the grid generation procedure. A standalone parametric geometry program built as a Matlab application is used to produce the rotor profile along with the vane at the initial rotor position. For a given set of rotor, stator diameters and number of vane with vane thickness, the program provide coordinate of the points on the chamber boundaries. This profile is an input to the meshing algorithm. Successive rotor positions appear to be rigid body rotations for the rotor while for the fluid volume that is deforming, it is a complex boundary motion where rotor rotates, stator is stationary and each of the vane is undergoing a general body motion. For simplification, blade tip clearance gap changes were not accounted in the presented analysis, but the meshing algorithm allows the possibility to further introduce a gap variation function.

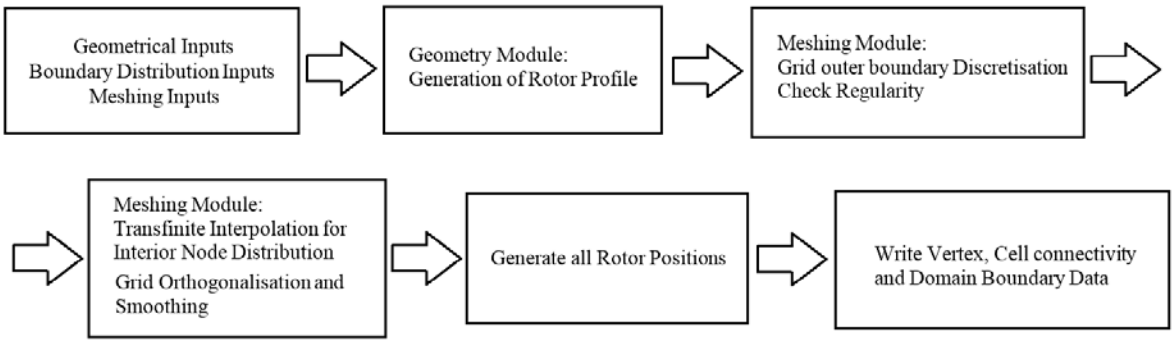

Figure 1. Vane geometry mesh generation procedure

The first stage in the meshing procedure is to discretize the boundaries. At this stage, inputs regarding the number of nodes and parameters for various control functions are taken from the user. The boundary discretization produces the distribution into the topology of an 'O' grid, as shown in Figure 2.b. An 'O' structure for the rotor mesh was purposely selected because it avoids any inaccuracies that can be introduced due to a non-matching mesh connection between core and leakage regions. The sudden transition from the leakage gaps to the core was handled by the introduction of stretching functions that gradually flare the radial mesh lines from leakage gap into the core as seen in Figure 2.c and Figure 2.d.

At the position where the core region topology does not remain rectangular, as it happens when the vane slides inside the rotor, a simplification has been introduced to convert the vane side walls into short segments on the rotor surface. It is anticipated that the leakage flow will not be influenced by this simplification as the gap clearance does not change but it significantly eases the O grid mesh generation.

The second stage in mesh generation is distribution of interior nodes. Transfinite interpolation, orthogonalisation and smoothing as described in [14] were used in these procedures to get a good quality hexahedral cell structure as seen in Figure 2.e. Once the 2D mesh is generated for all rotor positions, the mesh is assembled into 3D volume in the required format of the solver (Figure 2.f). In the current implementation there is possibility to export the mesh in solvers such as ANSYS CFX, ANSYS FLUENT, STAR CCM+ and Simerics PumpLinx. The entire meshing procedure was implemented in the software package SCORG™ developed at City, University of London [16].

The rotor domain is eventually connected to suction and discharge ports via non-conformal interfaces, as usually occurs in CFD analysis on positive displacement machines [12]. Ports meshing is usually carried out using standard tools and with reference to a tetrahedral cell structure to better capture the real geometry.

In the presented analysis, ANSYS CFX solver was used to calculate the oil injected flow fields in the air compressor in the first test case and a real gas fluid definition was used in the calculation of a ORC expander in the second test case. ANSYS CFX provides a model called Junction Box Routine that

is a user defined library to specify mesh deformation from custom applications such as SCORG. The solver updates the nodes coordinates from set of pre-generated coordinate files after every crank angle step (or its submultiples). Solver time step size finally results from the selected crank angle step and revolution speed of the rotor.

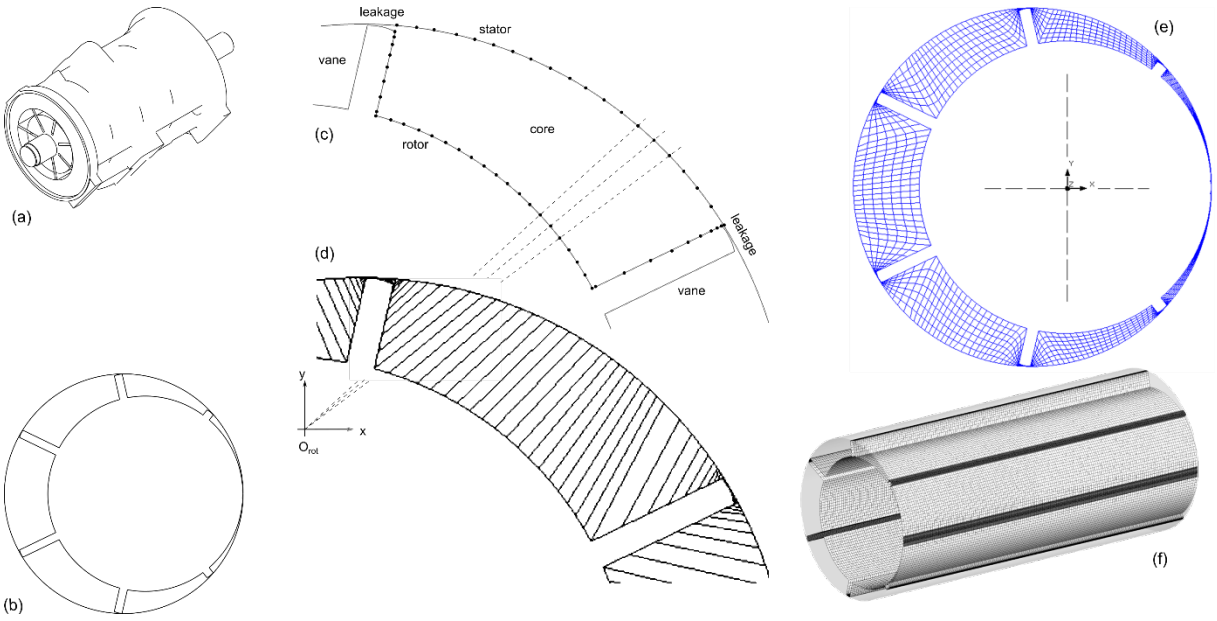

Figure 2. Grid generation procedure: (a) CAD drawing, (b) boundary generation, (c) boundary discretization, (d) stretching function applied to stator, (e) internal node distribution, (f) 3D grid

3. Numerical setups

Two test cases were analyzed using the new grid generation procedure developed in this work as represented in Table 1.

Table 1. Summary of geometrical and mesh specifics

	Oil injected Air Compressor		ORC Expander	
Rotor Diameter	195 mm		65 mm	
Axial Length	540 mm		60 mm	
Tip Clearance	50 µm		10 µm	
	Ports	Core	Ports	Core
Cell type	Tetrahedral	hexahedral	Tetrahedral	hexahedral
Node count (Million)	0.353	0.4735	0.135	0.157
Maximum aspect ratio	221	138	23	228
Minimum orthogonality	8.6	14.9	10.0	11.6

3.1. Case I: Oil injected air compressor.

The operating conditions that were considered as benchmark for the numerical results were 980 RPM as revolution speed and 8.70 bar_a as outlet pressure. Inlet pressure was 1.01 bar_a, inlet temperature 25.4 °C. The oil mass flow rate obtained from measurements was 2.9 kg/s and was used to specify the oil injection pressure so as to achieve this mass injection. Oil injection pressure was set at 6.6 bar_a, oil injection temperature was 65.0 °C. Under these conditions, the measurements showed that air mass flow

rate was 0.203 kg/s, compressor indicated power was 68.2 kW and shaft power recorder was 82.8 kW. Table 1 presents a summary of the geometry and CFD model mesh data for the case.

3.2. Case II: Real Gas, ORC application expander.

Table 1 also presents a summary of the geometry and CFD model mesh data for the expander case. From the tests performed in [17, 18], the operating conditions that were considered as benchmark for this case were 1551 RPM as revolution speed and 12.11 bar_a as inlet pressure with 90.5 °C as inlet gas temperature. Outlet pressure was 4.57 bar_a. Aungier Redlich Kwong (ARK) real gas model was used to specify the coefficients of the polynomials to define material properties and equation of state. Coefficients for specific heat and critical state temperature and pressure were supplied to generate a thermodynamic table in the temperature range of 273 and 400 K, while the pressure range was 2.0 and 60.0 bar_a.

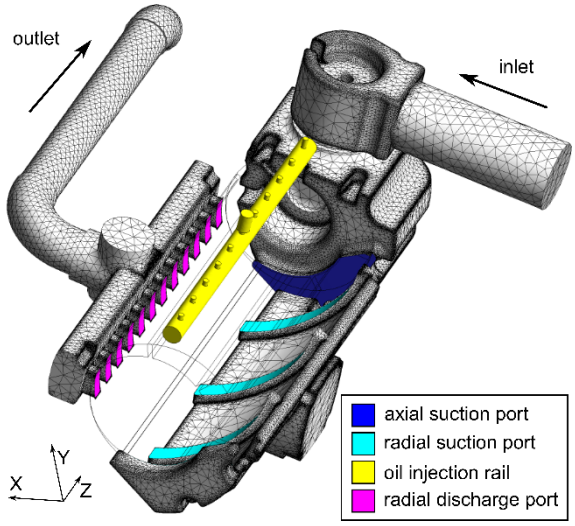

Figure 3. Compressor ports mesh

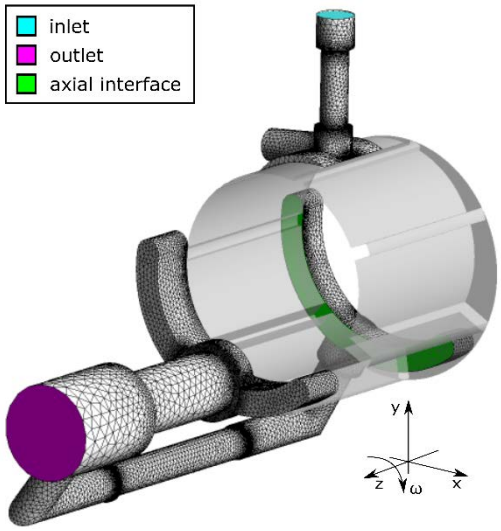

Figure 4. Expander ports mesh

Figure 3 shows the tetrahedral mesh used for the static ports of the oil injected compressor. Suction port, discharge port interface with the deforming rotor domain and the oil injection rail have been highlighted as in the colour scheme. Low pressure inlet and high pressure outlet boundaries are also seen. Similarly, Figure 4 represents the tetrahedral mesh used for the static ports of the real gas ORC expander. High pressure inlet, Low pressure outlet and the axial interface of low pressure port with the deforming rotor domain has been highlighted by the colour scheme. Radial interface of the high pressure port with the rotor is not seen. All these interfaces have been defined in the ANSYS CFX solver as non-conformal conservative flux type of fluid-fluid interfaces.

Table 2 presents the details of the CFD solver numerical setup. Most settings remained common between the two cases, except for the working fluid and solver relaxation parameters. Additionally since compressor case was solved as an oil injected flow, an eulerian-eulerian two phase solution was calculated. Air was the primary phase and constant density oil as liquid was set as the secondary continuous phase. Further details of oil injected compressor modelling can be found in Rane et al (2016). In terms of difficulty of solution, the compressor flow poses a challenge. In the compressor, the leakage flow through the tip gaps is in opposite sense to the main positive flow. Because of this and also due to the presence of oil phase, a gradual rise in discharge pressure was required to be specified. At the same time the solver relaxation factors were of lower order. On the other hand even though ARK real gas equation of state was defined with fixed table limits, a relatively easy convergence of the solver was observed. This could be due to the lower time step size and also the leakage flow sense in the same

direction as the main gas flow. A relatively higher solver relaxation factor could be specified in this case.

Table 2. Details on the numerical setups in the ANSYS CFX solver

	Air Compressor	ORC Expander
Mesh deformation	User defined nodal displacement via junction box routines in FORTRAN	
Mesh in ports	Tetrahedral with boundary layer refinements (Generated by ANSYS pre-processor)	
Turbulence model	SST – k Omega (Standard Wall Functions)	
Inlet boundary condition	Opening (Specified total pressure and temperature)	
Outlet boundary condition	Opening (Static pressure In case of backflow used as total pressure and temperature)	
Control volume gradients	Gauss divergence theorem	
Advection scheme	Upwind	
Pressure-Velocity coupling	Co-located layout (Rhie and Chow 4th order)	
Transient scheme	Second order (Fully implicit Backward Euler)	
Transient inner loop coefficients	Up to 20 iterations per time step	
Convergence criteria	r.m.s residual level 1e-03	
Working fluid	Air Ideal Gas + Liquid oil	R236fa (NIST coefficients ARK table)
Relaxation parameters	Solver relaxation fluids (0.1)	Solver relaxation fluids (0.4)

4. Results and Discussion

4.1. Case I: Oil injected air compressor.

Figure 5 reports the pressure contours in a cross section of the machine at 75 mm with respect to a full axial length of 540 mm. The sealing of the high pressure port from the suction port is apparent from the pressure distribution.

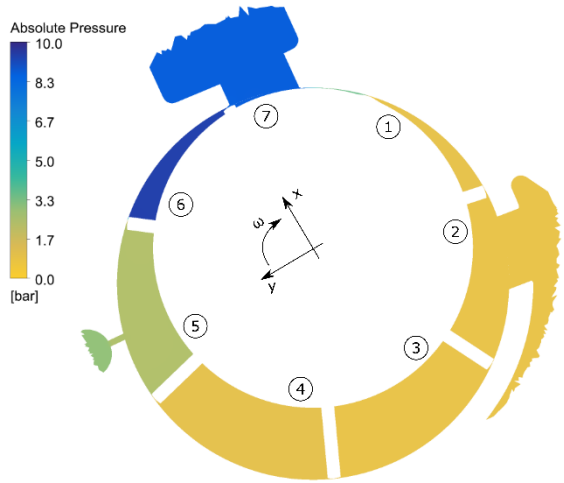

Figure 5. Compressor pressure - axial cross section at 14% of rotor length

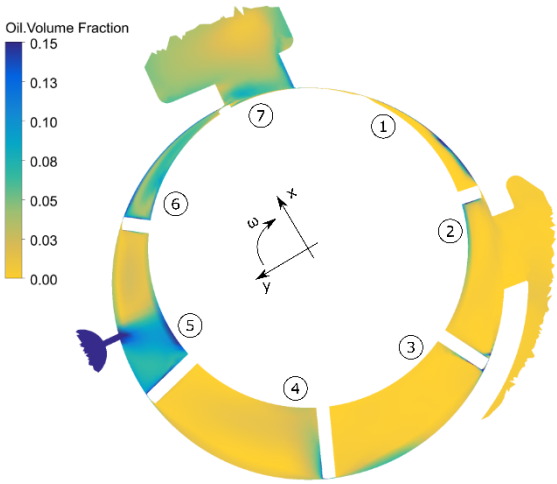

Figure 6. Compressor oil volume fraction - axial cross section at 14% of rotor length

The last 6th chamber is open to the discharge pressure of 8.7 bar_a but shows a slightly higher internal pressure of about 10.0 bar_a due to continued compression of the gas being discharged. Figure 6 reports the distribution of oil volume fraction in the same cross section at the same rotor position. From the leakage paths, oil is getting passed into the 1st suction chamber on the low pressure side. High oil concentration is visible in the injection rail and a radial jet of oil flow is visible in the 5th compression chamber. The pressure in this chamber is about 4.0 bar_a. About 6 – 8% oil volume fraction is observed in the discharge port.

Figure 7.a presents the distribution of gas temperature in this cross section while Figure 7.b is a 3D distribution of gas temperature with an oil iso-surface with 10% volume fraction superimposed in greyscale colors. Despite the sealing action of the lubricant, the clearance at the vane tip induces a backflow driven by adverse pressure gradient in opposite direction to the counter clockwise revolution speed sense in Figure 7.b. In turn, the overall flow field in the compressor vane is affected by a recirculation region whose magnitude is gradually lowered as the leakage flow interacts with the main one (which is aligned with the rotation sense). This phenomenon contributes to enhance the heat transfer between the compressing air and the oil that, after the radial injection shown in Figure 7.a, spreads along the leading side of the vane and mixes with air. The oil accumulation on the walls of the rotor, i.e. on the metallic surfaces which define the vane in reality, can be seen in the bottom left of Figure 7.b. These oil layers allow to lower friction losses between surfaces, namely stator with blade tip and blade side walls with rotor slots.

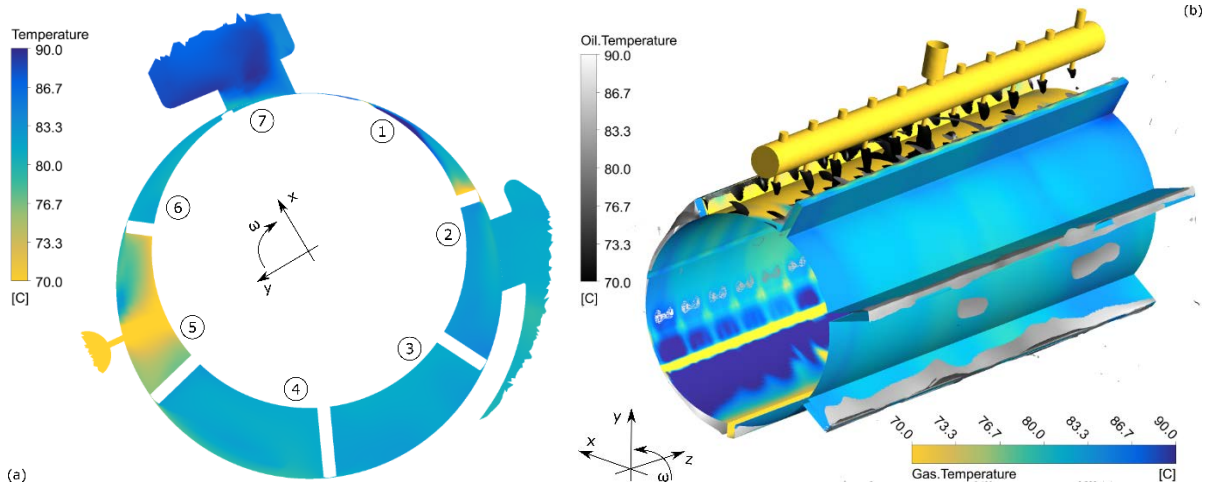

Figure 7. Compressor gas temperature: (a) cross section at 14% of rotor length, (b) 3D inner wall with injection rail and iso-surface having an oil volume fraction of 10%

4.2. Case II: Real Gas, ORC application expander.

Figure 8.a reports the pressure distribution of gas in case of the ORC expander simulation. Pressure from the high pressure port is at 12.11 bar_a and 90.5 °C. With expansion, a smooth decrease in gas pressure is visible across the chambers. Finally, pressure is at lower level of 3 bar_a from the 4th chamber onwards, when low pressure port is exposed. Figure 8.b represent the pressure distribution on the 3D rotor surface along with the vanes. A uniformity of pressure distribution is seen is individual chambers. Across the vane tip leakages, pressure gradients are observable. Similarly, Figure 9.a reports the gas temperature in the cross section and Figure 9.b presents gas temperature on the 3D rotor surface. In the cross section gradual reduction in gas temperature is visible. On the 3D rotor surface in chambers 1 and 2, a small non-uniformity of gas temperature distribution is seen due to the length of the intake port not covering the full rotor length and presence of axial low pressure ports on the two axial ends of the rotor.

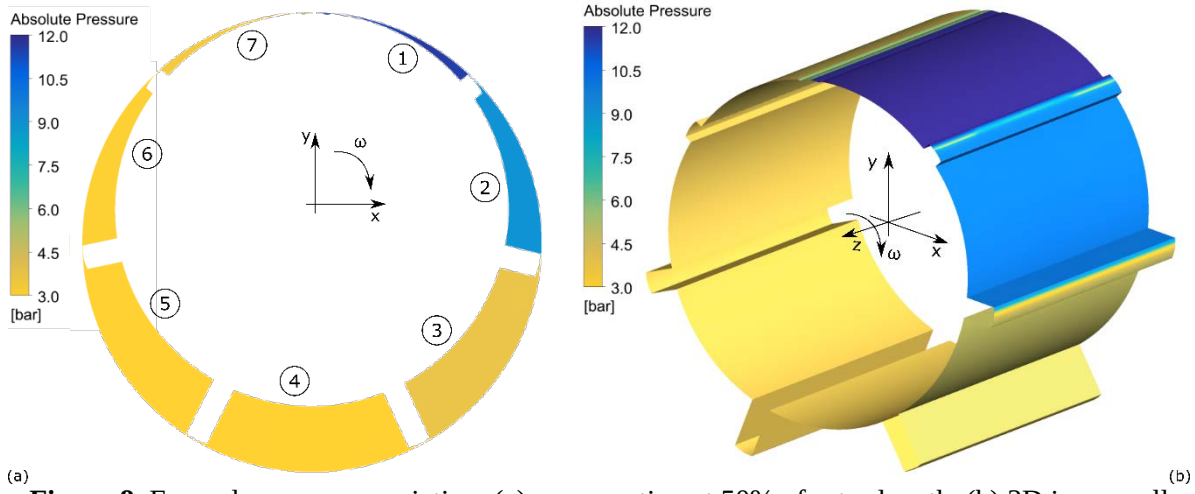

Figure 8. Expander pressure variation: (a) cross section at 50% of rotor length, (b) 3D inner wall

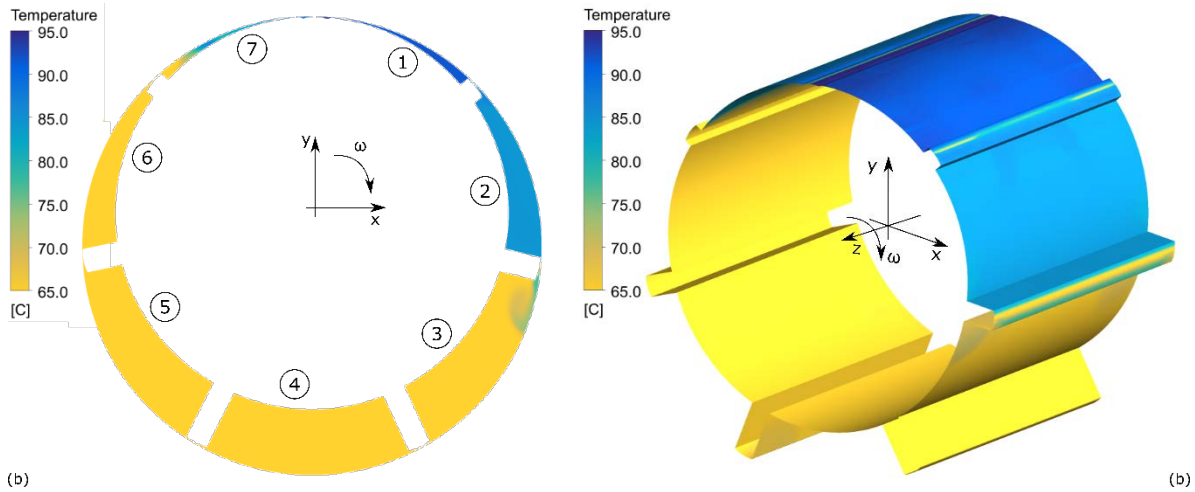

Figure 9. Expander gas temperature: (a) cross section at 50% of rotor length, (b) 3D inner wall

Table 3 presents the computational time required for generation of the grids using the developed algorithm and the time required by the CFD solver for calculation of a one boundary condition.

Table 3. Summary of computational time for grid generation and CFD calculations

	Oil injected Air Compressor		ORC Expander	
Generation for 720 positions				
2D cross section grid	120 seconds		120 seconds	
3D grid	900 seconds		720 seconds	
CFD solver computational time per case				
	Count	Time	Count	Time
Per time step	5 convergence iterations per step	700 seconds	3-5 convergence iterations per step	50 -55 seconds
Cyclically stabilised flow	1440 time steps	160 hours	1440 time steps	4 hours

5. Conclusions

The research work presented in this paper is the development of a robust and fast, deforming grid generation procedure for CFD analysis of sliding vane machines. Available literature suggested that only limited approaches to solving a full 3D numerical simulation in vane machines is currently available and the major limitation was found to be in the generation of deforming grids for the rotor domain. The developed grid and numerical methodology was eventually tested using the ANSYS CFX solver. Two vital test cases have been reported in the paper. First case is an industrial sliding vane oil injected air compressor and the second case is an ORC application, R236fa operated expander.

Multiphase simulations on the oil injected air compressor were successful in revealing the non-uniformity of gas temperature and oil distribution during the operation of the machine. Such a full scale model allowed to track a recirculation region induced in the vane flow field by the leakage flow through the clearance at the tip. Furthermore, the convective heat transfer with air showed the cooling capabilities of the lubricant even when supplied into the vanes as liquid jets. On the other hand, the oil temperature rise decreased its dynamic viscosity and, in turn, its hydrodynamic potential to prevent dry contact between blades and stator.

Real gas ARK model was successfully applied in the ORC expander analysis. The simulations provided information on the expander filling losses, internal expansion phenomenon and performance parameters could be evaluated at various operating conditions. Although due to the scope of this paper, flow results only from one of the selected operating conditions have been presented here.

These new procedures for grid generation of sliding vane machines will allow further design improvements and performance prediction of the machines with design modifications can be performed better. The effects of a variable tip clearance due to oil temperature and blade dynamics will be taken into account in future upgrades of the numerical methodology.

Acknowledgement

The work documented in this report has been funded by the 2015 Scholarship of the Knowledge Center on Organic Rankine Cycle technology (www.kcorc.org), the organization formed by the members of the ORC Power Systems committee of the ASME International Gas Turbine Institute (IGTI).

References

[1] O. Badr, S.D. Probert, P. O'Callaghan, Multi-vane expanders: Vane dynamics and friction losses, Applied Energy, Volume 20, Issue 4, 1985, Pages 253-285, ISSN 0306-2619, DOI:10.1016/0306-2619(85)90018-2.

[2] Tramschek, A. B., and M. H. Mkumbwa. Mathematical modelling of radial and non-radial rotary sliding vane compressors, International Compressor Engineering Conference at Purdue University, 1996, West-Lafayette (IN), United States, URL: docs.lib.purdue.edu/icec/1151/

[3] G. Bianchi and R. Cipollone, Theoretical modeling and experimental investigations for the improvement of the mechanical efficiency in sliding vane rotary compressors, Applied Energy, Volume 142, 15 March 2015, Pages 95-107, ISSN 0306-2619, DOI: 10.1016/j.apenergy.2014.12.055.

[4] G. Bianchi and R. Cipollone, Friction power modeling and measurements in sliding vane rotary compressors, Applied Thermal Engineering, Volume 84, 5 June 2015, Pages 276-285, ISSN 1359-4311, DOI: 10.1016/j.applthermaleng.2015.01.080

[5] Osama Al-Hawaj, Theoretical modeling of sliding vane compressor with leakage, International Journal of Refrigeration, Volume 32, Issue 7, November 2009, Pages 1555-1562, ISSN 0140-7007, DOI:10.1016/j.ijrefrig.2009.07.005.

[6] P. Kolasiński and P. Błasiak, Experimental and Numerical Analyses on the Rotary Vane Expander Operating Conditions in a Micro Organic Rankine Cycle System, Energies, Volume 9, 2016, ISSN 1996-1073, DOI: 10.3390/en9080606.

[7] G. Montenegro and A. Torre et al, Evaluating the Performance of a Rotary Vane Expander for Small Scale Organic Rankine Cycles Using CFD tools, Energy Procedia, Volume 45, 2014, Pages 1136-

1145, ISSN 1876-6102, DOI:10.1016/j.egypro.2014.01.119.
[8] Simerics PumpLinx, URL: www.simerics.com/pumplinx
[9] ANSYS CFX, URL: www.ansys.com/products/Fluids/ANSYS-CFX
[10] S. Rane, A. Kovacevic, N. Stosic, & M. Kethidi, (2013), Grid deformation strategies for CFD analysis of screw compressors, International Journal of Refrigeration, Volume 36, Issue 7, Pages 1883-1893, ISSN 0140-7007, DOI: 1016/j.ijrefrig.2013.04.008.
[11] S. Rane, Grid Generation and CFD analysis of Variable Geometry Screw Machines, 2015, PhD Thesis, City University London, URL: openaccess.city.ac.uk/id/eprint/15129.
[12] A. Kovacevic and N. Stosic and I. Smith, Screw Compressors - Three Dimensional Computational Fluid Dynamics and Solid Fluid Interaction, Springer, 2006, ISBN: 978-3-540-36302-6
[13] Vande Voorde, John, Jan Vierendeels, and Erik Dick. 2004. "A Grid Generator for Flow Calculations in Rotary Volumetric Compressors." In Proceedings of the Fourth European Congress on Computational Methods in Applied Sciences and Engineering.
[14] Kovačević A., 2005. Boundary Adaptation in Grid Generation for CFD Analysis of Screw Compressors, Int. J. Numer. Methods Eng., Vol. 64: 401-426.
[15] SCORG, URL: http://pdmanalysis.co.uk/
[16] S. Rane, A. Kovacevic, and N. Stosic, (2016), CFD Analysis of Oil Flooded Twin Screw Compressors, International Compressor Engineering Conference – Purdue. Paper 2392.
[17] R. Cipollone and G. Bianchi and D. Di Battista, et al., Mechanical Energy Recovery from Low Grade Thermal Energy Sources, Proceedings of the 68th Conference of the Italian Thermal Machines Engineering Association, Energy Procedia, Volume 45, 2014, Pages 121-130, ISSN 1876-6102, DOI: 10.1016/j.egypro.2014.01.014
[18] G. Bianchi, Exhaust Waste Heat Recovery in Internal Combustion Engines - Development of an ORC-based power unit using Sliding Vane Rotary Machines, 2015, ISBN 978-88-87182-69-9, DOI: 10.13140/RG.2.1.4095.7282 (PhD thesis)